Passive In-Slot Heat Path Realisation for Extending the Operating Limits of an Aircraft Propulsion Motor

Ahmed Hebala, Stefano Nuzzo, Peter H. Connor, Chris Gerada, Michael Galea

*[1]*Abstract*- **This paper studies the combined thermal and electrical characteristics of different in-slot conductive heat path materials and shapes to reduce the winding hotspot temperature and improve electrical motors' output power and performance. Combinations of analytical and 2D finite thermal models are developed and experimentally validated to consider the electromagnetic losses and temperature distributions within a slot-only model, as well as for a full motor. The models are used to assess a range of materials and operating conditions. The main parameters such as the thermal and electrical conductivity, and thickness of the in-slot passive heat conductive paths, are varied to generate a wider understanding of their operation for the future implementation of the heat path concept. Finally, the heat path is adopted for a high-performance aircraft propulsion motor to extend the operation limits. The analysis considered the thermal and electromagnetic aspects and the output power and power density have increased by 21% using the proposed heat path.**

Keywords- **Aircraft Propulsion, Electrical Machine Design, Heat Path, Thermal Management, Lumped Parameter Thermal Network.**

I. INTRODUCTION

The performance of electrical motors can be extended by integrating adequate cooling systems [1]. Nonetheless, the implementation of intrusive thermal management systems, such as spray cooling, stator flooding and cryogenic systems [2]-[5], can be challenging, due to their complexity and maintenance requirements. On the other hand, passive cooling systems such as embedded enhanced conductive heat paths (HPs) offer a promising solution for increasing electrical motor output power and power density, with minimum design variation and reduced risk of leakage in the slot [6]-[8]. Advancements in materials can also push electrical motor performance [9], [10]. In addition, thermal management systems improve motor reliability and fault tolerance [11]-[13]. In applications such as aerospace, the need for high efficiency, high reliability, and high-power density pushes the need to optimise all the electromagnetic, thermal, control, and mechanical aspects [14]-[18].

Currently, active liquid cooling is adopted in high-performance motors such as in [19]-[21]. Flooded or semi-flooded cooling approaches also offer effective thermal management but come with similar drawbacks [22], [23]. However, these techniques require significant sealing and parasitic pumping power, contrary to passive cooling approaches such as in-slot HPs.

A thermally conductive passive copper HP in the slot was introduced in [24] for a twelve-slot/ten-pole, double-layer wound, tubular linear PM motor. An LPTN model was developed with a total of 11 nodes inside the slot area. The results were validated also through thermal finite element method (FEM) software. The peak hot-spot temperature in the winding was significantly lowered from 180 °C to 110 °C, proving the success of this strategy in terms of slot temperature reduction [24]. In [25], computational fluid dynamics-based simulations were conducted to compare the thermal performance of two graphite-based materials with that of copper-based sheets. The simulations revealed that the graphite-based materials exhibited significant temperature reductions, averaging 40-50 °C lower than the copper-based sheets. This substantial decrease in temperature indicates that graphite-based materials could potentially offer superior thermal management in applications where heat dissipation is critical. However, it is important to note that these findings are based solely on simulations, with no experimental validation.

The authors in [6], [26] suggest extending a portion of the back-iron into the slot, which is a low-cost and practical technique to improve the thermal performance of electrical motors. This approach aims to improve heat dissipation, thereby reducing the peak winding temperature. However, this modification occupies some of the slot area, which can affect the motor's electromagnetic performance. Therefore, the thermal benefits of this technique must be carefully balanced against the potential drawbacks. An experimental test showed a 26.7% reduction in peak winding temperature for the same output power. A half-slot is modelled, which includes 25 nodes, with a 5 × 5 distribution to achieve a detailed temperature distribution. A thermal FEM model is also developed [6].

In the motor design process, electromagnetic and thermal elements are strongly related, making it inappropriate to adjust the motor shape solely for thermal reasons [6]. Thermal engineers need to ensure that the benefit of any suggested novel thermal technology is not offset by worsening other parameters, such as torque, and its quality, or motor losses.

This paper is dedicated to investigating the concept of passive conductive in-slot HPs, thus eliminating risks, complications and costs associated with liquid in-slot cooling.

This work is funded by the INNOVATIVE doctoral programme. The INNOVATIVE programme is partially funded by the Marie Curie Initial Training Networks (ITN) action (project number 665468) and partially by the Institute for Aerospace Technology (IAT) at the University of Nottingham.

Ahmed Hebala is with the Electrical and Control Engineering department, Arab Academy for Science, Technology and Maritime Transport, Alexandria, Egypt; ahmed.hebala@aast.edu.

Ahmed Hebala, Peter H. Connor and Chris Gerada are with the Power Electronics, Machines and Control (PEMC) Research Group, Faculty of Engineering, University of Nottingham, Nottingham, UK; ahmed.hebala@nottingham.ac.uk, peter.connor@nottingham.ac.uk, chris.gerada@nottingham.ac.uk.

Stefano Nuzzo is with the Department of Engineering Enzo Ferrari, University of Modena and Reggio Emilia, Modena, Italy; stefano.nuzzo@unimore.it

Michael Galea is with the Department of Electrical Engineering, University of Malta, MSD 2080 Msida, Malta; michael.d.galea@um.edu.mt.

The analysis also takes into account the performance and evaluation of different materials, shapes, and performance with an emphasis on aerospace electrical propulsion motors. Evaluation of the losses in the HP raised concerns about the operating limits and feasibility of the HP. In particular, the use of copper-based HPs could lead to excessive losses, even at low-frequency operations. Alternatively, an effective way to avoid large heat generation in the HPs is to employ alternative materials to copper.

This paper aims at experimentally evaluating a graphite sheet and a silicone-based sheet as T-shaped HP to extend the design boundaries and limits which are imposed by the copper-based HP losses. A lumped parameter thermal network (LPTN) and finite-element thermal models are developed as illustrated in Section II. An experimental setup is discussed in Section III, where the thermal performance of these sheets is compared to the performance of the baseline set by the copper HP. The practical results are presented and then used to validate the LPTN and FEM models. Then in Section IV, the losses in the HP are evaluated for the tested materials and the thermal performance is reevaluated based on the generated losses in the HP. Additionally, a generic study that sweeps a wide range of material thermal and electrical conductivities is carried out to extend the work further as carried out in Section V. Finally in Section VI, utilising the understanding of the HP performance, an aircraft propulsion motor case study is presented by implementing the optimal HP to increase the output power and power density. Ultimately, the conclusions are laid out in Section VII.

II. HP Description and Thermal LPTN and FE Model

Four motorettes were manufactured and tested in this study. One motorette (Moto 1) has no HP, while in the rest a 'T' shaped HPs are included. Ideally, the HPs should have all been identical in thickness. However, off-the-shelf market availability dictated the specific material and dimension combinations selected for this research study. Nevertheless, custom material sizes can be commissioned for high-volume production.

The main parameters for Moto 2, 3 and 4 are listed in Table I and shown in Fig. 1. The axial stack length of motorettes is 151 mm. The first motorette (Moto 1) is the baseline case without a HP. A side view of the prototyped motorette is shown in Fig. 2, where cooling channels, windings, HP, and thermocouple leads can be observed. Furthermore, thermal nodes, thermocouple's locations and materials matching with Moto 1 is illustrated in Fig. 3. Additionally, temperatures in Moto1 were measured by 31 thermocouples, while 29 thermocouples were used for measuring temperatures in Moto 2-4, covering the various regions and layers of the winding and the motorette as a whole. The sides of the motorettes have an adiabatic boundary condition to simulate the symmetry between neighbouring slots as shown in Fig. 3.

The second motorette (Moto 2) has an HP made from copper sheets. Thus, it is a conventional material compared to Moto 3 and 4. The copper sheet is believed to be the best performing thermally, as it has a high isotropic thermal conductivity of 390 W/mK. However, the thermal performance is limited by the losses generated. Thus, Moto 3 and 4 are being proposed for comparison and extension of the scope of the analysis.

Table I:
HP properties.

Motorette ID	Moto 2	Moto 3	Moto 4
HP Material	copper	graphite	silicone-gel
Max. operating temperature (°C)	450	400	200
Dimensions			
Width, Length – XY – (mm)	50 – 151	50 – 151	50 – 151
Thickness – Z – (mm)	1.12	0.4	1.0
XY-thermal conductivity (W/mK)	390	400	13
Z-thermal conductivity (W/mK)	390	28	13
XY-thermal resistance per unit	1.00	2.73	33.60
Z-Thermal resistance per unit	1.00	4.89	26.35

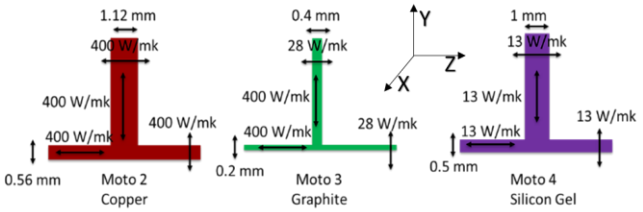

Fig. 1: HP sheets dimensions and thermal conductivities.

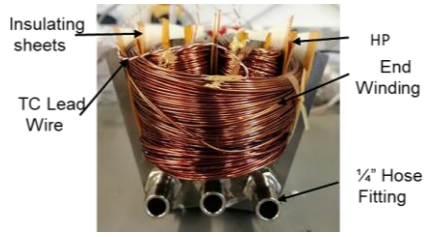

Fig. 2: Side view of a motorette showing the end windings.

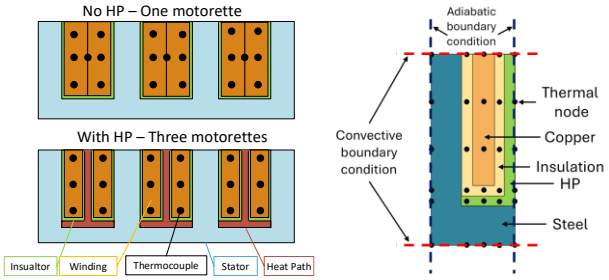

Fig. 3: Half-slot model of the motorette with 30 thermal nodes.

The third test piece (Moto 3) HP is made from a thin sheet of low thermal resistance graphite thermal interface material (Panasonic, EYGS1316ZLAC). This specific type is typically used for cooling electronic devices such as IGBT modules, motor control units, and servers. It is manufactured in sheets less than 0.5 mm in thickness. For this experiment, the thickest one available was 0.2 mm. It has an anisotropic thermal conductivity of 400 W/mK in the plane (the XY-direction), and only 28 W/mK through the plane (Z-direction). Nevertheless, this is at least two orders of magnitude higher than resin and has a similar thermal conductivity to steel.

The last motorette (Moto 4) has an HP made from a sheet of alumina-silicone-gel (RS-Components product number '707-4774), thus it will be referred to as silicone-gel hereafter. It has a uniform thermal conductivity of 13 W/mK. The selected sheet has a thickness of 0.5 mm.

The graphite and silicone-gel-based sheets (Moto 3 and 4) were selected as they possessed the competitive market readiness potential to the copper HP in terms of thermal and electrical conductivity, as well as other advantages such as lighter weights and higher flexibility.

LPTN and FE models are built to represent the slot and HP thermal behaviours. The models and experimental results are

used to cross-validate each other in Section III, and the models are then used for further design sensitivity investigations in Section IV.

The main 30-node LPTN model is shown in Fig. 3. The in-slot insulation thickness is 0.15 mm and has a thermal conductivity of 0.2 W/mK. The effective winding thermal conductivity within the slot is calculated based on (1) [27].

$$k_{eq} = k_{imp} \frac{(1+FF)\,k_{cu} + (1-FF)\,k_{imp}}{(1-FF)\,k_{cu} + (1+FF)\,k_{imp}} \quad (1)$$

In (1), FF is the slot fill factor, and k_{imp} is the conductivity of the resin impregnation. The winding equivalent thermal conductivity is 1.1314 W/mK assuming a fill factor of 0.45. The loss is distributed radially across the slot area.

The thermal 2D FE model for the four motorettes is developed. The temperature map and heat flow at 300 W are depicted in Fig. 4. The model used for the graphite sheet considers the anisotropic nature of the thermal conductivity.

III. EXPERIMENTAL TESTING OF ADVANCED HP MATERIALS

This section gives a comprehensive account of the HP experimental testing. A description of the test setup details is provided, followed by a detailed results analysis and discussion.

a. *Experiment setup and test procedures*

The testing setup and diagram are shown in Fig. 5. A temperature control unit (Tool Temp, model TT-188) is used to maintain a steady cooling fluid temperature, and a water-to-air chiller (from TECARC, model XC1000) was used to cool down the temperature control unit. A flow meter (Hydrotechnik, model number CVC05W3B-A353) was used to monitor the flow rate, through two ball control valves for bypass and motorette flow control. The whole motorette, as well as the main pipes, were wrapped with a thermally insulating blanket cover to minimise losses to the environment. A controlled DC power supply (From EA-PS, model EA-PS 9360-40) was connected to the terminals of the windings in power control mode, and the three coils are connected in series.

The tests were performed on each motorette individually. The testing range for the flow rates was between 2 to 12 litres/min. For each test, the flow rate was initially set at the maximum flow rate (12 litres/min) and the power supply was set at an initial power of 100 W until it reached a thermal steady-state. This process was then repeated in increasing power increments of 50 W until the maximum temperature recorded reached approximately 180 °C. The cycle was then repeated with reducing flow rates in steps of 2 litres/min. This method ensures a full flow and power matrix of tests below the winding temperature limit. Each test lasted between 25-45 minutes.

The steady-state condition was defined in this context when the temperature variation was less than 1 °C for at least 5 minutes. Steady-state voltage, current, whole winding resistance and temperatures were recorded.

b. Experimental results

This section contains a description and discussion of the thermal test results. For brevity, the 12 litres/min results are presented, and the Moto 1 (non-HP design) is used as the baseline case for comparison.

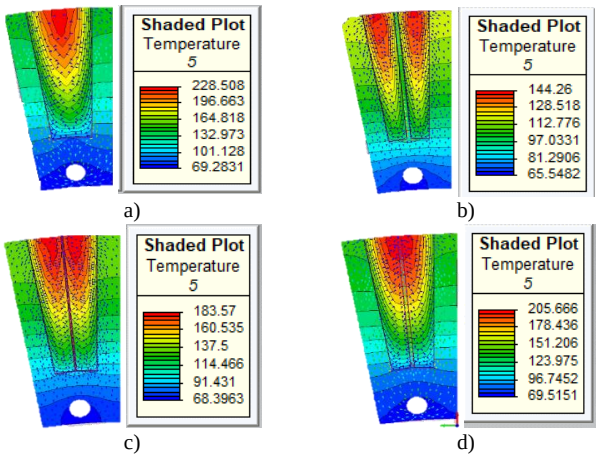

Fig. 4: Thermal FE model temperature map at 300 W, a) No HP (Moto 1), b) Cu HP (Moto 2), c) Gr HP (Moto 3), d) silicone-gel HP (Moto 4).

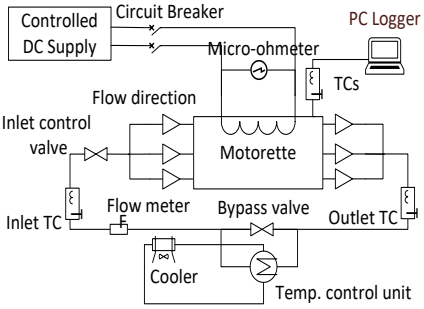

Fig. 5: Experimental testing setup diagram.

Figure 6(a) shows the winding maximum and average temperature reduction for the three motorettes. Regarding the hot spot temperature reduction, indeed Moto 2 with the copper heat path is still the leading option, with up to 60 °C reduction being achieved. The graphite HP achieved the maximum decrease recorded at 31.5 °C. Even though the silicon-gel material had the lowest internal thermal conductivity compared to the other materials, it managed to reduce the average winding temperature by 10.1 °C and the hotspot temperature by 15.8 °C, as shown in Fig. 6(a). A 15.8 °C temperature reduction is a considerable amount in many applications, especially considering that it generates no losses compared with copper and graphite.

In Fig. 6(b) the radial temperature gradient across the slot depth is studied, and the results represent the temperature difference between the motorettes with HPs and the Moto 1 (no HP). Each layer temperature is the average of six TCs distributed in the three slots of one motorette.

It is evident from this analysis that Moto 2 with the copper HP is superior in thermal performance. Indeed, the copper-based HP can reduce the slot top layer temperature up to 57 °C. These reductions are more than double that of Moto 3 with the graphite sheets. In fact, the silicone-gel HP can barely reduce the temperature at the top layer, and practically increases the middle layer temperatures by up to 9% to 11%, depending on the flow rate. The bottom layer performance across different motorettes is quite similar between the three motorettes The graphite HP maximum temperature reduction is 26.1 °C at 12 litres/min at the top layer and the bottom layer.

The experimental results are compared to those of the LPTN and FE models in Fig. 7. Both FE and LPTN results match the

experimental data well, enabling extended analysis in future investigations.

The FE results showed similar trends to the LPTN model as exemplified in Fig. 7. Overall, these differences are in an acceptable range, considering the difficulty of matching the same boundary conditions such as the exact flow rate, the convective heat transfer coefficient and perfect thermal insulation. As well as further practical manufacturing uncertainties including sensor contact, impregnation quality and material contact quality.

The second Motorette has a very good matching between the LPTN and the experimental results, as depicted in Fig. 7. The average absolute and relative difference at 12 litres/min is approximately 3 °C and 3% respectively. The overall agreement between the LPTN and the experimental results for the copper-based HP are in an acceptable range. It can also be noted that compared to the first motorettes, more points of comparison are available since Moto 2 was able to withstand higher power loss input.

The LPTN model for the graphite HP motorette compared with the experimental results possesses very high accuracy at 12 litres/min. Indeed, the average difference is -1.5 °C as well as an average relative difference of 11.5%. This motorette is more challenging to model as it has an anisotropic thermal conductivity as previously stated. The average temperature of the winding of Moto 4 also showed a good match with the experimental results. At 12 litres/min, the difference is from -1.3 °C to -2.3 °C.

Therefore, this robust and adaptable LPTN gives the confidence to push forward in the research of considering other design variations.

IV. HP ELECTROMAGNETIC LOSSES

A critical aspect that may be overlooked is assessing the electromagnetic and thermal inter-dependent effects of the HP. In this section, the losses that may be generated in the HP are computed through full-scale transient electromagnetic 2D simulation. At first, the electrical conductivity of the HP materials is experimentally measured. As these are off-shelf materials, the detailed electromagnetic characteristics are not known, particularly for graphite and silicone sheets. Then, the losses are assessed at different operating frequencies, to represent different motor operating speeds. Afterwards, these evaluated losses are added to the LPTN model to fully evaluate the HP more thoroughly.

a. HP loss quantification

A sheet resistivity meter 'Nagy SD-800' uses the four-point measurement technique to measure the material values as illustrated in Fig. 8. The graphite sheet has a sheet conductivity of 26-30 mΩ/Square, which for a 0.2 mm sheet thickness is equal to 1.67e5 Siemens/m (0.287% IACS). The silicone-gel sheet on the other hand is identified by the properties as an insulating material. The copper sheet electrical conductivity is set to 5.77e7 Siemens/m.

The frequencies explored range from 21 Hz to 672 Hz, which represent the typical operating frequency range for the application at hand. The ratio between the winding losses and the losses generated in these sheets is quantified through FE simulations and plotted in Fig. 9. The losses generated in these

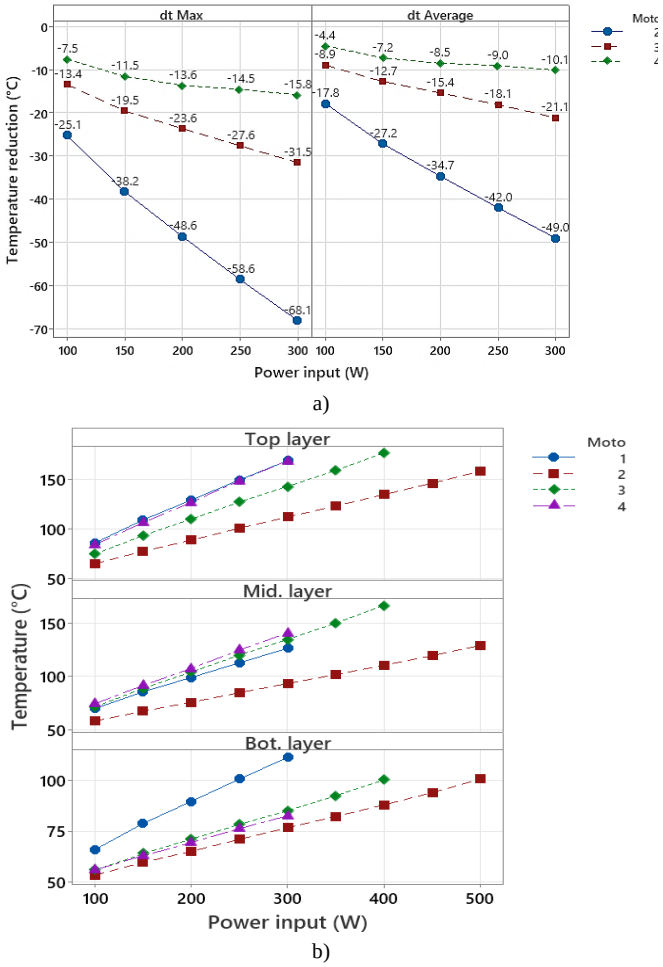

Fig. 6: Winding temperature, a) Winding's average and hotspot temperature reduction, b) different layers temperatures.

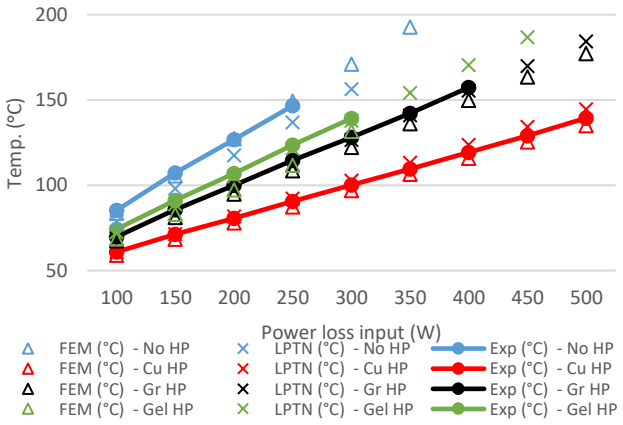

Fig. 7: Experimental, LPTN model and FEM verification at 12 litre/min.

sheets are quantified through an electromagnetic FE transient simulation as shown in Fig. 10.

It is evident that the copper-based HP losses reach quite substantial values even at very low frequencies, for example at 21 Hz it reaches a quarter of the winding losses, and at 672 Hz it reaches almost 24.7. Therefore, loss mitigation should be taken into account when designing these HPs such as HP segmenting or slicing to prevent high eddy current losses.

Whereas the losses in Moto 3, where the graphite sheet is used, maintain a relatively low ratio (HP to Winding losses) up to 0.21 at the 336 Hz mark and reach a maximum loss ratio of

0.36 at 672 Hz. Due to availability, the graphite sheets were notably smaller in thickness when doing the experimental testing. Therefore, a modified sheet is simulated to have the same thickness as the copper-based sheet to enable a fair comparison, showing a very similar pattern as before.

The losses in the silicone-based sheet (Moto 4) remain zero for all operating conditions, therefore no further evaluation is added here.

b. Accounting for the HP losses

The eddy current losses quantified above are used in the LPTN model to evaluate the use of a specific HP material in a motor.

The performance of the copper HP was very promising in terms of temperature reduction for the same winding loss input as discussed earlier. Indeed, it can result in a temperature difference of up to 60 °C. However, it also produces losses equal to a quarter of the winding losses at frequencies as low as 21 Hz. Therefore, as depicted in Fig. 11(a), the copper-based HP is only acceptable up to operation at very low frequencies sub 20 Hz – which limits its practical implementation without significant modification of the HP such as segmentation. However, it still can be viable for motors operating at low rotational speeds and frequencies.

Furthermore, plotted as reference lines the performance of the same motorette without accounting for the HP losses, the silicone-based one, and the motorette without a HP.

On the other hand, the performance of the graphite sheet is illustrated in Fig. 11(b). The graphite sheet should be thermally effective up to 448 Hz, but only up to 336 Hz when comparing the performance to the silicone-based sheet. The temperature increase due to the losses up to the 112 Hz range is marginal. Hence, the Graphite HP is still thermally beneficial for this application. Therefore, it has an extended operating range when compared to the copper HP.

V. EXTENDED HP MATERIALS STUDY

The aim of this section is to formulate an understanding of the behaviour of a wider and more generic range of materials and properties. The electrical conductivity is varied and the losses generated at different frequencies are quantified.

a. Generic sensitivity analysis

The electromagnetic (EM) FE model was used to quantify the losses generated in the HP at different speeds (frequencies) and at the full range of the electrical conductivity from 0.001 to 100 %IACS.

The results are in Table II, where a list of the ratio between the losses in the HP to the winding losses is reported. Up to 0.1 %IACS the loss in the HP is minimal even at higher frequencies. In fact, at 21 Hz, if the material is fully electrically

conductive, it might still be thermally beneficial if the thermal conductivity is high, such as copper (Moto 2).

b. Other suggested materials

A more realistic and pragmatic approach is to consider other materials that it was not possible to acquire and test practically.

A comprehensive list of 56 materials was considered to this purpose. Two main criteria are used to select these materials. First, it must have a continuous operating temperature of at

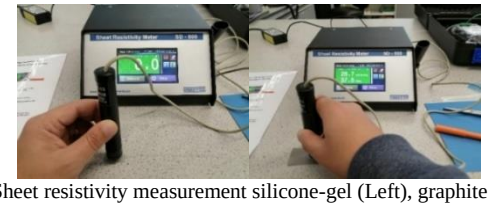

Fig. 8: Sheet resistivity measurement silicone-gel (Left), graphite (Right).

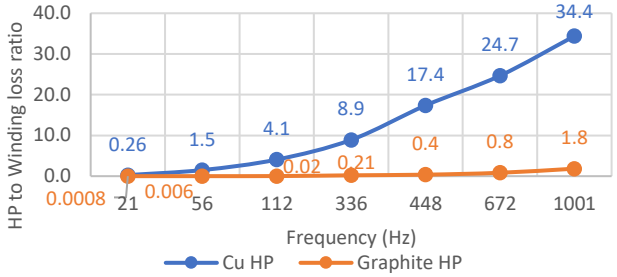

Fig. 9: Ratio of HP losses to winding losses for copper and graphite sheets.

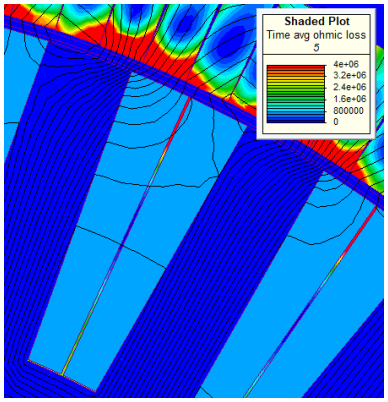

Fig. 10: Time-averaged ohmic losses plot at 336 Hz for the graphite sheet.

a)

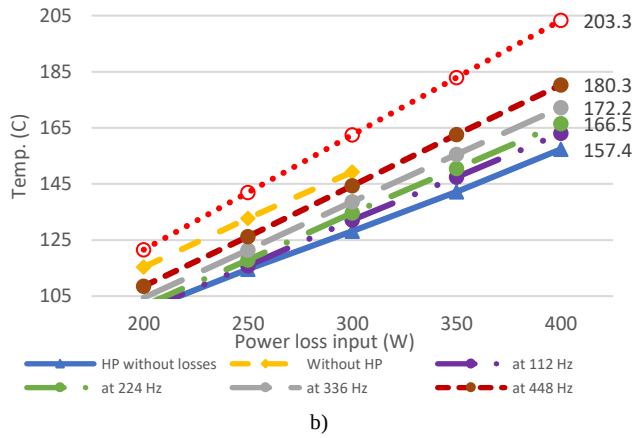

b)

Fig. 11: Average temperatures with HP losses , a) copper, b) graphite.

least 180 °C. Secondly, the thermal conductivity should be at least 20 W/mK.

The selection should also take into account the density and the price in addition to the thermal and electrical conductivities and the temperature limit. These lists are generated with the help of CES software [28].

It must be mentioned that the software does not list the thermal conductivity through different planes, therefore, the values used assume that all these materials have uniform thermal conductivity. For example, carbon fibre would have lower thermal conductivity through the thickness of the sheets, due to the lower thermal conductivity of the resins that it used to manufacture these sheets [29]. Hence, the assessment of performance should take all these factors into account.

The average and maximum temperature for the winding when using all these materials as the HP is plotted against the thermal conductivity are shown in Fig. 12. The simulations are performed for the same motorette design, at 12 litres/min and at 300 W losses.

The two performance indices reach a knee at around 50 to 150 W/mK. This is a crucial conclusion that can be used as a guide when selecting an HP sheet material.

VI. IMPLEMENTING THE HP FOR A PROPULSION MOTOR

The proposed HP shapes and materials are considered for a propulsion motor (ProMo) as a means of extending the thermal and electromagnetic performance by mean of a combined thermal and electromagnetic simulation. In this section, the concept of HP is implemented to further improve the ProMo performance. The main performance of the ProMo is discussed, and a full account is reported in [30].

a. ProMo EM performance and HP adaptation framework

This motor design is for an aircraft propulsion application. It is based on improving an existing reference electrical device for a commercial aircraft such as the Cessna Caravan, which carries 8-12 passengers [31]. Enhanced thermal and electrical performance standards have been established, with the full details of the design being available in [30]. It was possible to achieve the required output power of 550 kW, and a low torque ripple of 0.4% without skewing.

The motor temperatures are kept within the thermal limits by the designed water jacket cooling system, without direct winding cooling or shaft liquid cooling in the motor shaft. The motor benefits from an open slot design, that eases the winding and manufacturing procedures and is advantageous for the HP. The motor has four sets of three-phase windings hence improving the motor fault tolerance. A summary of the main motor parameters is listed in Table III.

The HP is introduced to the ProMo through a generic sensitivity analysis to evaluate its general feasibility. Secondly, an appropriate HP size for the ProMo slot area is explored. Thirdly, the losses generated in the HP are evaluated for the three different HP materials (copper, graphite and silicone-gel) as previously investigated in Section II, but this time implemented for six different HP shapes. Finally, the combined effect of the HP on the thermal and magnetic performance of the ProMo is explored. It is worth mentioning that the results reported in the next subsections are based on FE simulations of the ProMo,

Table II:
HP to winding losses ratio range varied by electrical conductivity and operating frequency.

Conductivity	Frequency (Hz)			
%IACS	21 Hz	56 Hz	112 Hz	224 Hz
0.001	2.3E-06	1.9E-05	6.5E-05	3.1E-04
0.010	2.3E-05	1.9E-04	7.6E-04	3.1E-03
0.100	2.3E-04	2E-03	6.5E-03	0.03
1.000	2.3E-03	0.02	0.065	0.30
10.000	0.02	0.19	0.625	2.82
100.000	0.21	1.43	3.37	8.17

Table III:
ProMo Main Design Features and Parameters.

Parameter	Value	Parameter	Value
Stator Lam Dia (mm)	435	Slots/Poles	72/22
Tooth Width (mm)	7.8	Output Power (kW)	555
Slot Depth (mm)	38	Power Density (kW/kg)	6.12
Slot opening (mm)	7	Efficiency (%)	98.5
Axial Length (mm)	142	Current density (A/mm2)	9.5

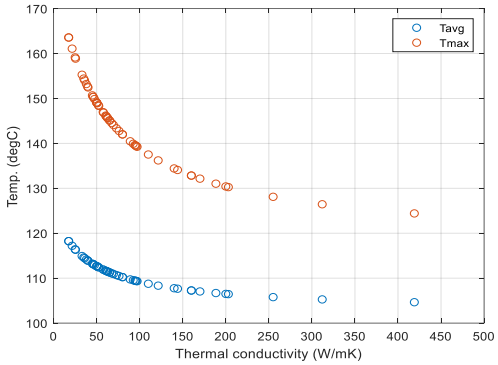

Fig. 12: Average and maximum temperature for a wide range of HP materials' thermal conductivity.

b. Generic HP model with no HP losses

A sensitivity analysis of the HP design is conducted to evaluate the overall performance of the HP with the ProMo. The main parameters of the sensitivity study are the HP width and radial and tangential thermal conductivity. In addition, the six proposed HP shapes are considered as an additional design variation, as reported in Fig. 13(b). For this purpose, a generalised 55-node thermal network as shown in Fig. 13(a) is developed, which can be adopted for all the six HP shapes by adjusting the proper thermal resistance parameters.

The width is varied from 0.2 mm to 2 mm, and the thermal conductivities are varied from 5 W/mK to 400 W/mK. The baseline design is set at 180 ˚C in the case with no HP. Thus, the heat input is set at this level and then the temperature drop is evaluated with the presence of the HPs.

The results for the average temperature reduction defined by different ranges of HP thermal conductivity are shown in Fig. 13. It is evident from the result that the radial thermal conductivity of the HP is a major contributor to high-temperature reduction. The gradient is substantial for lower values, whereas starting from 200 W/mK the increase in the thermal conductivity has a very minimal effect on the temperature reduction.

A scatter plot of the peak temperature based on the HP width and the radial thermal conductivity is plotted in Fig. 14. A linear relationship exists, such that thicker HPs lead to a higher reduction of temperature.

An interesting finding from Fig. 15 is that the cross (tangential/circumferential) thermal conductivity gives almost the same response as long as it exceeds the limit of 5 W/mK.

Hence, it is concluded that any material candidate for the HP should have a cross-thermal conductivity of at least 5 W/mK, and 200 W/mK for the radial thermal conductivity.

Shape B has the highest temperature reductions, following it are shapes D and F, whereas the lowest reductions are from shape E. Additionally, it is noted that the variation of performance is minimised at a width higher than 0.5 mm.

c. Updating the winding area

The HP takes up space from the winding area, thus it can be a limiting factor when selecting the size of the HP. Ideally, thicker HPs are more advantageous but that would lead to less space for the windings, hence higher DC losses. The ProMo was designed with a high fill factor. Therefore, it is challenging to add an HP with a large width. To accommodate an HP in the slots, a smaller wire cross-section could be used, or a lower number of strands as two of the least intrusive methods possible. On the other hand, a redesign of the slot area and the stator could be carried out as well, but this is less favourable at this stage.

The adopted method to include the HP is by reducing the strand cross-section. Several options were considered. Eventually, a 0.6 mm HP was opted for, and the diameter of the strands was reduced from 15.5 AWG to 16 AWG. As a result, the phase resistance increased, and copper losses increased from 4.2 kW to 4.8 kW (14.3%). Therefore, any HP fitted in the slot should overcome this increase in power losses and reduce the overall slot temperature. Additionally, the HP losses should be considered, as pursued in the next subsection.

d. Combined thermal and EM effects of the HP

The losses generated in the HP are calculated by integrating the HP in the EM FE model and simulating the motor in a transient environment. The ProMo fundamental frequency at 2000 rpm is 366.67 Hz. The ohmic losses for shape B are shown in Fig. 16 as an example of the analysis. The three materials experimentally tested in Section II are tested in this analysis, which are copper, graphite and silicone-gel sheets. The electrical conductivity is 99.5% IACS, 0.3% and 0% for the three materials respectively. The six shapes proposed are shown in Fig. 13 and Fig. 14.

The copper HP has some detrimental effects on the performance of the ProMo. The torque ripple is increased by at least tenfold, and the output power is also reduced. More predominantly, the HP losses are very high, for all the HP shapes except for 'E'. On average, the HP losses are ten times higher, so any expected thermal benefits from these HPs would be opposed by the high HP losses. Nevertheless, the losses induced in shape 'E' are much lower than the losses generated in the other HP shapes. The main reason for these lower losses in the 'E' HP, is being away from the slot opening and higher flux density areas in the slot. This aspect can be interesting such

as that of shortening and pushing away from the slot opening for the HPs of the other five shapes.

The losses generated in the graphite HP are averaged at 11% of the winding losses. The overall EM performance of the motor is virtually the same as without the HP. The silicone-gel HP,

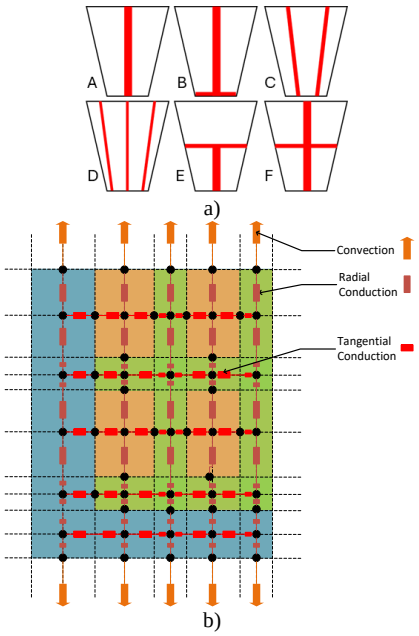

Fig. 13: Proposed generic LPTN half-slot node locations. a) the proposed six HP, b)shapes generic 55-Node LPTN network.

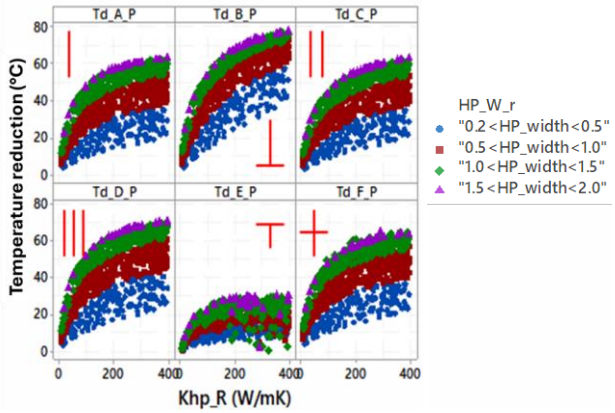

Fig. 14: Scatter plot of temperature reduction of the ProMo with the HP width and radial thermal conductivity as variables for six HP shapes.

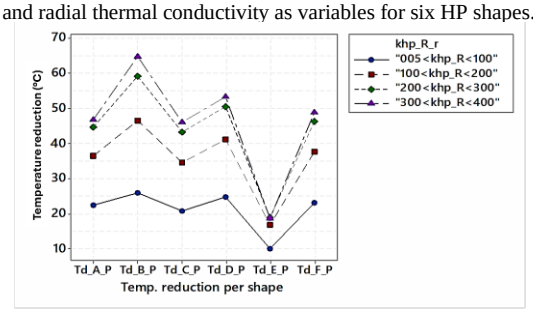

a) HP radial thermal conductivity

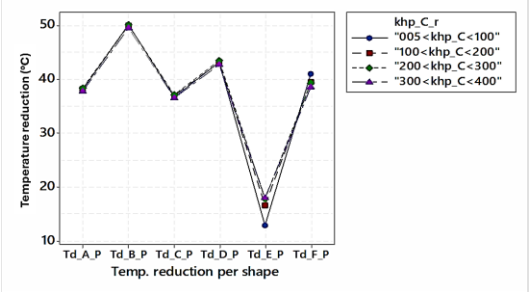

b) HP tangential thermal conductivity

Fig. 15: Average temperature reduction of the ProMo at different conditions no HP losses included.

however, generated no losses; therefore, the electromagnetic performance is practically unchanged with or without the HPs.

Thus, the copper HP is excluded from the analysis since the losses generated in the HP are far greater than those within the winding. The thermal performance of the graphite and the silicone-gel HP are evaluated.

e. Extending the ProMo operating limits

As there is a temperature reduction in the winding, the phase current can be increased to increase the motor's output power. Thus, at an HP width of 0.6 mm, the phase current and the heat loss input are continuously increased and the EM and thermal models are coupled to evaluate the performance. The aim is to keep increasing the winding heat loss input until the temperature of the winding reaches the thermal limit of 180 ˚C.

This process is applied to both the graphite and silicone-gel materials and for all the six HP shapes and compared to the slot with no HP. The results are shown in Fig. 17. The Y-axis shows the winding peak temperature and the X-axis lists both the phase current and the corresponding motor output power.

The silicone gel had a maximum temperature reduction of 12 ˚C, thus the maximum increase of current occurs with HP shape 'B' at 226 A, which leads to an increase of 15 kW in the output power. Although there are no losses generated in the HP, the thermal and EM gains are very minimal due to the relatively low thermal conductivity (13 W/mK).

The graphite-based HP of shape 'B' can push the current up to 276.6 A, reaching the windings' thermal limit. The main performance indicators are listed in Table IV. The proposed motor incorporating the HP has a power output of 671 kW compared to the based design of 556 kW, thus an increase of 21.0%.

This 21.0% increase in output is significant and could open opportunities for other applications. On the negative side, the torque ripple has increased from 0.4% to 1.1%, yet this is still acceptable for this application. Additionally, the efficiency has settled at 98.0% compared to 98.4% earlier. This is mainly due to the increase of winding losses caused by the phase current, and the addition of the losses from the HP. Nevertheless, a 0.4% drop in efficiency is justified as the propulsion output power has increased by 21.0% and the power density has reached 7.4 kW/kg.

Consideration of the weight and the cost of the HP are also recommended for a full-picture evaluation of the HP. For example, considering the full motor, the weight of the copper HP would be 2.73 kg and the graphite alternative is only 0.62 kg since the density is 8933 kg/m^3 and 1900 kg/m^3 for copper and graphite, respectively. Therefore, the overall weight of the motor would be decreased by 2.11 kg, which can be very valuable in aerospace applications.

VII. CONCLUSION

This paper has investigated the effectiveness of slot HPs using various materials, quantified the losses generated in these HPs, and applied this knowledge to enhance the performance of an aircraft propulsion motor.

The experimental and simulation results demonstrate that copper-based HPs offer the most significant temperature reductions (up to 80-100°C), but their effectiveness is limited at higher frequencies due to electrical losses. Graphite HPs, while less effective than copper at low frequencies, are suitable for operation up to 336 Hz and provide reductions of 50-60°C. Silicone-gel HPs, being electrically non-conductive, consistently provide a cooling effect of 10-20°C.

By incorporating graphite HPs into the stator slots, a 21% increase in output power and power density was achieved in the propulsion motor used as case study in this paper. This improvement is attributed to the enhanced heat dissipation capabilities of graphite, which outweighs the added weight and reduced slot fill factor. However, its mechanical durability and potential degradation under continuous or intermittent load conditions need to be evaluated to fully assess its applicability in aerospace scenarios. These studies will be addressed in future work, along with different machine design approaches to better host the optimal HP shape, such as ad-hoc slot-tooth layouts, etc.

Table IV:
Performance of the ProMo with HP Shape B.

	ProMo (No HP) at 220 A	ProMo with a graphite HP shape B at 276 A
Average Torque (Nm)	2653	3220
Torque Ripple (%)	0.4	1.1
Pout (kW)	556	674 (+21.0%)
Efficiency (%)	98.4	98.0
Power density (kW/kg)	6.1	7.4 (+21.0%)
Magnet Losses (W)	3381	3662
HP Losses (W)	0	1086
Winding Losses – W)	4179	4818
Rotor Losses (W)	136	151
Stator Losses (W)	968	1009
Winding Max. Temp. (ºC)	182.0	180.0

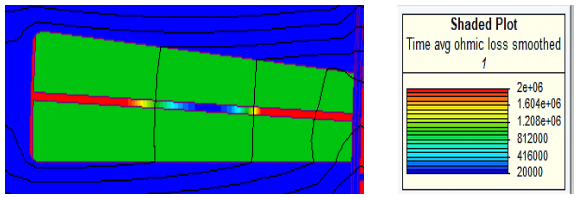

Fig. 16: Ohmic losses of the HP in the ProMo for graphite HP shape B.

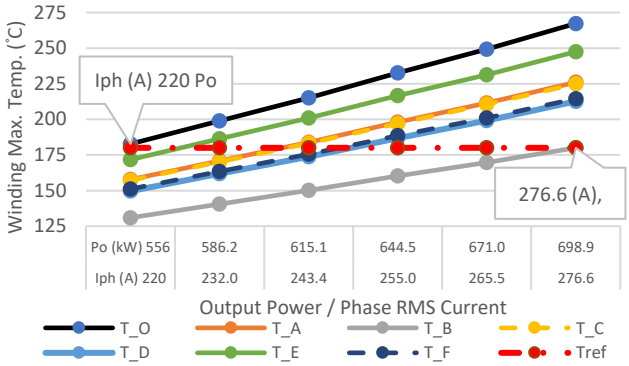

a) graphite HP

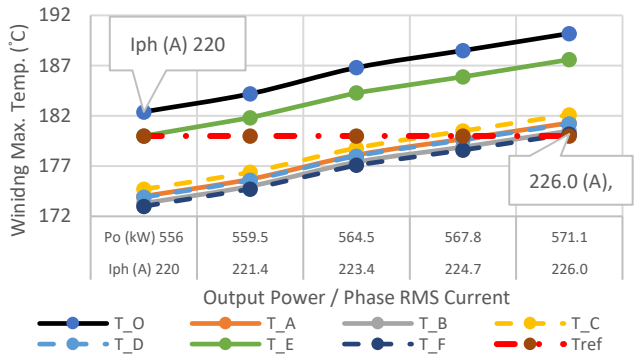

b) silicone-gel HP

Fig. 17: Output power and current increase by using the HPs.

REFERENCE

[1] A. La Rocca *et al.*, "Thermal management of a high speed permanent magnet machine for an aeroengine," *Proceedings - 2016 22nd International Conference on Electrical Machines, ICEM 2016*, pp. 2732–2737, 2016, doi: 10.1109/ICELMACH.2016.7732908.

[2] C. Liu *et al.*, "Experimental Investigation on Oil Spray Cooling with Hairpin Windings," *IEEE Transactions on Industrial Electronics*, vol. 67, no. 9, pp. 7343–7353, 2020, doi: 10.1109/TIE.2019.2942563.

[3] A. Al-Timimy *et al.*, "Design and Losses Analysis of a High Power Density Machine for Flooded Pump Applications," *IEEE Trans Ind Appl*, vol. 54, no. 4, pp. 3260–3270, 2018, doi: 10.1109/TIA.2018.2821623.

[4] Z. Xu *et al.*, "A semi-flooded cooling for a high speed machine: Concept, design and practice of an oil sleeve," *Proceedings IECON 2017 - 43rd Annual Conference of the IEEE Industrial Electronics Society*, vol. 2017-Janua, no. October, pp. 8557–8562, 2017, doi: 10.1109/IECON.2017.8217503.

[5] Y. Terao, W. Kong, H. Ohsaki, H. Oyori, and N. Morioka, "Electromagnetic Design of Superconducting Synchronous Motors for Electric Aircraft Propulsion," *IEEE Transactions on Applied Superconductivity*, vol. 28, no. 4, pp. 4–8, 2018, doi: 10.1109/TASC.2018.2823503.

[6] F. Zhang *et al.*, "Back-Iron Extension Thermal Benefits for Electrical Machines with Concentrated Windings," *IEEE Transactions on Industrial Electronics*, vol. 67, no. 3, pp. 1728–1738, 2020, doi: 10.1109/TIE.2019.2903758.

[7] S. Ayat, R. Wrobel, J. Goss, and D. Drury, "Experiment informed methodology for thermal design of PM machines," *2016 11th International Conference on Ecological Vehicles and Renewable Energies, EVER 2016*, pp. 1–7, 2016, doi: 10.1109/EVER.2016.7476428.

[8] R. Wrobel, P. H. Mellor, M. Popescu, and D. A. Staton, "Power loss analysis in thermal design of electrical machines," *Proceedings - 2015 IEEE Workshop on Electrical Machines Design, Control and Diagnosis, WEMDCD 2015*, pp. 118–126, 2015, doi: 10.1109/WEMDCD.2015.7194519.

[9] H. Liu, S. Ayat, R. Wrobel, and C. Zhang, "Comparative study of thermal properties of electrical windings impregnated with alternative varnish materials," *The Journal of Engineering*, vol. 2019, no. 17, pp. 3736–3741, 2019, doi: 10.1049/joe.2018.8198.

[10] A. Cavallini, D. Fabiani, and G. C. Montanari, "Power electronics and electrical insulation systems - Part 2: Life modeling for insulation design," *IEEE Electrical Insulation Magazine*, vol. 26, no. 4, pp. 33–39, 2010, doi: 10.1109/MEI.2010.5511187.

[11] S. H. Basha and S. Chakravorty, "A new approach to perform accelerated reliability testing of low tension motors," *Reliability: Theory & Applications*, vol. 8, no. 4 (31), pp. 75–83, 2013.

[12] J. Nandan and R. Gobbi, "High reliability for electric machines driving critical loads: A review," *2011 IEEE Applied Power Electronics Colloquium, IAPEC 2011*, pp. 132–137, 2011, doi: 10.1109/IAPEC.2011.5779849.

[13] A. Hebala, S. Nuzzo, P. H. Connor, C. Gerada, and M. Galea, "On the Fault Tolerance and PM Demagnetisation of a High-Performance Aircraft Propulsion Motor," in *2022 International Conference on Electrical Machines, ICEM 2022*, 2022. doi: 10.1109/ICEM51905.2022.9910866.

[14] A. Hebala, S. Nuzzo, P. H. Connor, P. Giangrande, C. Gerada, and M. Galea, "PM Halbach Arrays in Motors: Loss Reduction and Performance Improvements," *23rd International Conference on Electrical Machines and Systems, ICEMS 2020*, pp. 710–715, 2020, doi: 10.23919/ICEMS50442.2020.9291234.

[15] Z. Xu, M. Galea, C. Tighe, T. Hamiti, C. Gerada, and S. J. Pickering, "Mechanical and thermal management design of a motor for an aircraft wheel actuator," *2014 17th International Conference on Electrical Machines and Systems, ICEMS 2014*, pp. 3268–3273, 2014, doi: 10.1109/ICEMS.2014.7014056.

[16] B. Silwal, A. H. Mohamed, J. Nonneman, M. De Paepe, and P. Sergeant, "Assessment of different cooling techniques for reduced mechanical stress in the windings of electrical machines," *Energies (Basel)*, vol. 12, no. 10, 2019, doi: 10.3390/en12101967.

[17] B. Zhang, R. Qu, X. Fan, and J. Wang, "Thermal and mechanical optimization of water jacket of permanent magnet synchronous machines for EV application," *Proceedings - 2015 IEEE International Electric Machines and Drives Conference, IEMDC 2015*, pp. 1329–1335, 2016, doi: 10.1109/IEMDC.2015.7409234.

[18] A. Hebala, S. Nuzzo, P. H. Connor, G. Volpe, C. Gerada, and M. Galea, "Analysis and Mitigation of AC Losses in High Performance Propulsion Motors," *Machines*, vol. 10, no. 9, 2022, doi: 10.3390/machines10090780.

[19] L. John, S. Reuter, D. Becker, H.-C. Möhring, R. Eisseler, and M. Doppelbauer, "Prototype fabrication of complex cooling channels by potting, additively manufactured inserts in an electric motor," in *2023 13th International Electric Drives Production Conference (EDPC)*, Nov. 2023, pp. 1–6. doi: 10.1109/EDPC60603.2023.10372147.

[20] L. John, S. Haehnlein, S. Reuter, M. Doppelbauer, and L. F. Berg, "Resource-efficient integration of slot cooling channels in a hairpin electric motor," in *Elektromechanische Antriebssysteme 2023; 9. Fachtagung (VDE OVE)*, Nov. 2023, pp. 294–298.

[21] Z. Yao, R. K. Mandel, and F. P. McCluskey, "In-slot Cooling for High Power Density Electric Motor with Encapsulation Channels," in *2022 21st IEEE Intersociety Conference on Thermal and Thermomechanical Phenomena in Electronic Systems (iTherm)*, May 2022, pp. 1–6. doi: 10.1109/iTherm54085.2022.9899559.

[22] Z. Xu *et al.*, "A semi-flooded cooling for a high speed machine: Concept, design and practice of an oil sleeve," *Proceedings IECON 2017 - 43rd Annual Conference of the IEEE Industrial Electronics Society*, vol. 2017-Janua, no. October, pp. 8557–8562, 2017, doi: 10.1109/IECON.2017.8217503.

[23] R. Wang, X. Fan, D. Li, R. Qu, L. Li, and T. Zou, "Convective Heat Transfer Characteristics on End-Winding of Stator Immersed Oil-Cooled Electrical Machines for Aerospace Applications," *IEEE Transactions on Transportation Electrification*, vol. 8, no. 4, pp. 4265–4278, Dec. 2022, doi: 10.1109/TTE.2022.3186800.

[24] M. Galea, C. Gerada, T. Raminosoa, and P. Wheeler, "A thermal improvement technique for the phase windings of electrical machines," *IEEE Trans Ind Appl*, vol. 48, no. 1, pp. 79–87, 2012, doi: 10.1109/TIA.2011.2175470.

[25] Z. Xu, C. Tighe, M. Galea, T. Hamiti, C. Gerada, and S. J. Pickering, "Thermal design of a permanent magnetic motor for direct drive wheel actuator," *Proceedings - 2014 International Conference on Electrical Machines, ICEM 2014*, pp. 2186–2192, 2014, doi: 10.1109/ICELMACH.2014.6960487.

[26] F. Zhang, D. Gerada, Z. Xu, H. Zhang, and C. Gerada, "Equivalent Slot Thermal Conductivity and Back-iron Extension Effects on Machine Cooling," *2019 22nd International Conference on Electrical Machines and Systems, ICEMS 2019*, 2019, doi: 10.1109/ICEMS.2019.8921725.

[27] A. Zeaiter, M. Fenot, and D. Saury, "Numerical Approach to Determining Windings' Thermal Conductivity," *Proceedings - 2018 23rd International Conference on Electrical Machines, ICEM 2018*, pp. 1291–1296, 2018, doi: 10.1109/ICELMACH.2018.8506692.

[28] "CES EduPack software, Granta Design Limited, Cambridge, UK, 2009."

[29] M. Liu, Y. Li, H. Ding, and B. Sarlioglu, "Thermal management and cooling of windings in electrical machines for electric vehicle and traction application," *2017 IEEE Transportation and Electrification Conference and Expo, ITEC 2017*, pp. 668–673, 2017, doi: 10.1109/ITEC.2017.7993349.

[30] A. Hebala, S. Nuzzo, P. H. Connor, P. Giangrande, C. Gerada, and M. Galea, "Improved propulsion motor design for a twelve passenger all-electric aircraft," *Proceedings - 2021 IEEE Workshop on Electrical Machines Design, Control and Diagnosis, WEMDCD 2021*, pp. 343–348, 2021, doi: 10.1109/WEMDCD51469.2021.9425667.

[31] A. Hebala *et al.*, "Feasibility Design Study of High-Performance, High-Power-Density Propulsion Motor for Middle-Range Electric Aircraft," *IEEE International Symposium on Industrial Electronics*, vol. 2020-June, no. 665468, pp. 300–306, 2020, doi: 10.1109/ISIE45063.2020.9152551.

Ahmed Hebala (M'23) received his PhD from the University of Nottingham in 2023, and he received the BSc and MSc degrees in Electrical Engineering from the Arab Academy for Science, Technology and Maritime Transport, Alexandria, Egypt in 2013 and 2017 respectively. In January 2018, he was appointed a Marie Curie Early-Stage Research Fellow and a PhD candidate at the University of Nottingham.

He worked as an assistant lecturer for three years and is currently an Assistant Professor at the Electrical and Control Engineering Department at the AAST.

His main research interests include the design and optimization of electrical machines, thermal management of electrical machines, renewable energy sources, process automation and robotics. He serves as an Associate Editor for the Robotics Integration, Manufacturing and Control (RIMC) Journal.

Stefano Nuzzo (M'18) received his PhD degree in Electrical and Electronic Engineering in 2018 from the University of Nottingham, Nottingham, U.K, where he also worked as a Research Fellow within the Power Electronics, Machines and Control (PEMC) Group. He is currently an Assistant Professor in Electrical Machines and Drives at the Department of Engineering "Enzo Ferrari" of the University of Modena and Reggio Emilia, Modena, Italy. His research interests are the analysis, modelling and optimizations of electrical machines intended for power generations, industrial and transport applications.

He is the Secretary of the Electrical Machines, Drives and Automation Committee (TC3) of the IEEE Power Electronics Society (PELS). Also, he serves as Area Editor for the IEEE Transactions on Transportation Electrification and as Associate Editor for the IEEE Transactions on Energy Conversion.

Peter H. Connor received the M.Eng. and Ph.D. degrees from the Department of Mechanical, Materials and Manufacturing Engineering, University of Nottingham, Nottingham, U.K., in 2009 and 2014, respectively. He is a Senior Research Fellow with the Power Electronics, Machines and Control Research Group, Faculty of Engineering, University of Nottingham.

His research interests are mechanical design and thermal management of electrical machines for industrial power generation and high-speed, high power-density traction, and aerospace applications.

Chris Gerada (M'05-SM'12) received the Ph.D. degree in numerical modelling of electrical machines from The University of Nottingham, Nottingham, U.K., in 2005. He subsequently worked as a Researcher with The University of Nottingham on high-performance electrical drives and on the design and modelling of electromagnetic actuators for aerospace applications. Since 2008, he was appointed as a Lecturer and since 2013, as a Professor at The University of Nottingham. His main research interests include the design and modelling of high-performance electric drives and machines.

Michael Galea (M'13-SM'18, FRAeS) received the Ph.D. degree in electrical machines design in 2013 from the University of Nottingham, Nottingham, U.K. He was promoted to Full Professor of Electrical Machines and Drives with the University of Nottingham in 2019. Since 2021, Prof Galea is with the Department of Electrical Engineering of the University of Malta. His main research interests include design and development of electrical machines and drives (classical and unconventional), reliability and lifetime degradation of electrical machines and the more electric.